lubricants

MDPI

Article

Control of Active Magnetic Bearings in Turbomolecular Pumps for Rotors with Low Resonance Frequencies of the Blade Wheel

Markus Hutterer * and Manfred Schrödl

Institute of Energy Systems and Elektrical Drives, TU Wien, Gusshausstr. 25, 1040 Vienna, Austria; manfred.schroedl@tuwien.ac.at

* Correspondence: markus.hutterer@tuwien.ac.at; Tel.: +43-588-0137-0237

Received: 30 May 2017; Accepted: 19 July 2017; Published: 25 July 2017

Abstract: Rotors with high gyroscopic effects and low resonance frequencies caused by the blade wheel (blade frequencies) can lead to stabilization problems in the application field of turbomolecular pumps. If such a rotor is stabilized by active magnetic bearings, the control structure could be destabilized by the splitting up of the rigid body eigen-frequencies caused by the gyroscopic effect. The control structure of the magnetic bearings can also destabilize the eigen-modes caused by the blade wheel, if the gain of the control structure is too high in the range of the eigen-frequencies of the blade wheel. To deal with the problem of the gyroscopic effect, a decoupling and compensation method was developed based on the inverse dynamics of the rigid body rotor. The gain of the control structure in the range of the blade frequencies is decreased using a Kalman filter. To increase the damping of the system, the predicted states of the linear magnetic bearing model using a Kalman filter are applied instead of the sampled values of the sensors directly. For the decoupled structure, PID controllers are used for stabilization. The functionality of the control structure is verified by a measurement of the current and position signal using the Kalman states and the sensor values. The robustness and performance in the frequency range are verified using the sensitivity and compliance function.

Keywords: magnetic bearing; gyroscopic effect; turbomolecular pump; Kalman filter

1. Introduction

Magnetic bearings are used if an almost friction-less or wear-less operation is required. In this context, active magnetic bearings (AMBs) are used with increased regularity. In many applications of turbomolecular pumps, lubricant should be avoided. Therefore, active magnetic bearings are sometimes unavoidable for the rotor stabilization in this application field. The mechanical behavior of AMBs can be changed during operation. This feature allows an optimization of the rotor running behavior dependent on the operating point. AMBs use electro-magnets for force generation, instead of permanent magnets, which are used in passive magnetic bearings. However, to decrease the losses in AMBs, also permanent magnets (PMs) can be used for pre-magnetization [1,2]. AMB systems are unstable for open loop operation, and a feedback controller is required for a stable levitation. To close the feedback loop, the position information of the rotor is required. In many applications, this information is provided by different kinds of sensors. However, also self-sensing methods exist, where the actuator itself is used to detect the rotor position [3,4]. An AMB system is a nonlinear multiple input and multiple output (MIMO) system. A decentralized control is a quite straightforward method, because the proportional part can be interpreted as a spring and the derivative part as a damper [5]. However, the coupling terms of the system description are not considered in the design procedure. As a consequence, the tilting and translation modes cannot be treated independently from each

other, and the gyroscopic effect couples the motions of the tilting movements. In [6–8], decoupling approaches are used based on the inverse dynamics to decouple the system and compensate the impact of the gyroscopic effect on the rigid body movement. In [9–14], modern control approaches, such as H∞ and μ-synthesis control theory, were used. Due to the non-linear nature of AMBs, the use of linear time-invariant (LTI) controllers could lead to problems. In [15,16] a nonlinear feedback linearization based on differential geometric methods was used to solve this problem. Also sliding mode controller can be used to overcome the nonlinear nature of AMBs [17]. However, many applications of magnetic bearings have a sufficient linear behavior, which allows the use of linear controllers. In many cases, the dynamic simulation is only done using beam elements, where the eigen-dynamics of the blade wheel is neglected. For such non-modeled effects in combination with the dynamic behavior of the control structure, complicated modern control approaches could be difficult to adjust. In contrast, proportional–integral–derivative (PID) controllers have a straightforward design procedure, and the mechanical behavior is easily adapted. Thus, the main share of industrial applications is based on PID controllers.

This paper deals with a control algorithm, which is based on the inverse dynamics of the system for the decoupling and compensation of the gyroscopic effect. For the decoupled system, a decentralized PID controller is developed. Compared to the gain schedule of the decentralized PID controller, this method compensates the parameter variant gyroscopic effect. Thus, the separating margin between the bending modes and the rigid body modes can be kept constant for a high speed range. The investigated rotor has low blade resonance frequencies, which lie near the operating range. Therefore, a Kalman filter is designed to decrease the gain of the control structure in the range of the blade resonance frequencies. Using the proposed control structure, the rotor could be prevented from destabilization caused by the blade frequencies. The functionality and robustness of the proposed control structure are shown in experimental results.

The contributions of the present paper can be summarized as follows:

- A decoupled control procedure is developed for a magnetically-levitated rotor with low blade frequencies
- The gain of the control structure is significantly reduced in the frequency range of the blade frequencies using a Kalman filter for the feedback of the tilting movement. Without the Kalman filter, the system becomes unstable above a certain speed.

The paper is organized as follows. In Section 2, the basic system equations of the radial movement of a five-degree of freedom (5-DOF) magnetic bearing system is explained. Section 3 explains the development of the control structure and describes the most important parameter to stabilize the magnetic levitated rotor. Section 4 states the main results of the control structure applied on a turbomolecular pump. Section 5 summarizes the conclusions of the paper.

2. Modeling of a 5-DOF AMB System

A 5-DOF AMB system consists of two radial bearings and one axial bearing according to Figure 1. In many industrial applications of active magnetic bearings, the axial movement is not coupled with the radial movement for the controller design. In this case, the axial movement can be interpreted as a single input and single output (SISO) linear time-invariant (LTI) system. Especially for small displacements of the rotor compared to its size, the decoupled approximation is sufficient. The control of a SISO AMB system using a PID controller was already described in [18]. Therefore, the aim of this paper is the control of the radial movement. An AMB applies forces on the rotor. Thus, no kinematic constraint has to be fulfilled for the rotor. For such a system, the Euler equations can be used directly for the rotational movement. For a general body, the Euler equations are given in a body fixed reference frame, because of the constant matrix of inertia. However, in the case of rotational symmetric rotors,

the matrix of inertia is also constant in a non-body fixed frame. The Euler equations in a non-body fixed frame are given as:

$$\boldsymbol{\Theta}\dot{\boldsymbol{\omega}} + \boldsymbol{\Omega} \times (\boldsymbol{\Theta}\boldsymbol{\omega}) = \mathbf{M} \tag{1}$$

where $\boldsymbol{\Omega}$ is the angular velocity vector of the chosen coordinate system, $\boldsymbol{\omega}$ is the angular velocity vector of the body, $\boldsymbol{\Theta}$ is the moment of inertia matrix and $\mathbf{M}$ is the torque vector. The translation movements are described using Newton's law. The stabilized rotor in this paper is assumed to be rotationally symmetric. 5-DOF are stabilized by AMBs, and only the rotation around the z-axis is controlled by an electrical motor with an independent speed controller. The equations of motion of the radial movement are described in a reference frame, which is the same as the body fixed, but without a rotation around the z-axis. Under the following assumptions [19]:

- The rotor is symmetric and rigid
- The displacement of the rotor is small compared to its dimensions
- The angular velocity ω is assumed to be constant

the equations of motion are given as:

$$\mathbf{M}\ddot{\mathbf{x}} + \mathbf{G}(\omega)\dot{\mathbf{x}} = \mathbf{F} \tag{2}$$

with:

$$\mathbf{M} = \begin{bmatrix} I_x & 0 & 0 & 0 \\ 0 & m & 0 & 0 \\ 0 & 0 & I_x & 0 \\ 0 & 0 & 0 & m \end{bmatrix} \quad \mathbf{G}(\omega) = \begin{bmatrix} 0 & 0 & I_p\omega & 0 \\ 0 & 0 & 0 & 0 \\ -I_p\omega & 0 & 0 & 0 \\ 0 & 0 & 0 & 0 \end{bmatrix} \quad \mathbf{F} = \begin{bmatrix} M_\beta \\ F_x \\ M_\alpha \\ F_y \end{bmatrix} \quad \mathbf{x} = \begin{bmatrix} \beta \\ x_S \\ \alpha \\ y_S \end{bmatrix} \tag{3}$$

where I_x is the equatorial moment of inertia, I_p is the polar moment of inertia, m is the mass of the rotor, the entries of $\mathbf{F}$ are the forces or torques of each degree of freedom and the entries of $\mathbf{x}$ are the degrees of freedom according to Figure 1. Equation (2) describes the basic mechanical equation of a supported rotor. The system equation for different bearing structures lies in the calculation of the force vector $\mathbf{F}$. For the magnetic bearing, a dominant magnetic field can be assumed in many cases. The electromagnetic force can be calculated with:

$$\mathbf{F}_m = \int_{\partial V} \frac{1}{\mu_0} \left(\mathbf{n} \cdot \mathbf{B}\mathbf{B} - \frac{1}{2} B^2 \mathbf{n} \right) dS \tag{4}$$

where ∂V is a closed surface, which includes the considered body, μ_0 is the permeability of free space, $\mathbf{n}$ is the normal vector of the chosen surface and $\mathbf{B}$ is the flux density. For many magnetic bearing systems, the normal vector $\mathbf{n}$ and the flux density vector $\mathbf{B}$ are assumed to be collinear. If the flux density $\mathbf{B}$ in the air gap is additionally assumed to be constant in space, the force can be calculated using the following algebraic equation.

$$\mathbf{F}_m = \frac{A_p}{2\mu_0} |B|^2 \mathbf{n} \tag{5}$$

with the surface of the pole area A_p. Equation (5) can be interpreted as a basic equation for calculating the force generation of magnetic bearings. The different structures and different geometries of active magnetic bearings differ only in the calculation of the magnetic flux $\mathbf{B}$. Figure 2 shows two common structures of AMBs.

Because the magnetic force depends on $|B|^2$, the forces at the pole areas can only pull the rotor. To overcome that problem, a bias flux I_b is used. If a resulting force should act in a specified direction, the flux is increased in the pole area of this direction and decreased in the opposite using a control current I_x or I_y. Thus, a resulting force is generated in the requested direction, although every single force in the pole areas pulls on the rotor. Magnetic bearing structures using the differential driving mode have only one coil for each pole. The bias current I_b and the control current I_x or

I_y are superposed to the required coil current. Therefore, every degree of freedom requires two current controllers. For the differential winding mode, the bias flux is generated with separated coils. Therefore, the control flux can be created with only one current controller for every degree of freedom. In [2,3,20], the bias flux is generated by permanent magnets. Such a magnetic bearing structure is called a permanent magnet biased active magnetic bearing (PMBAMB).

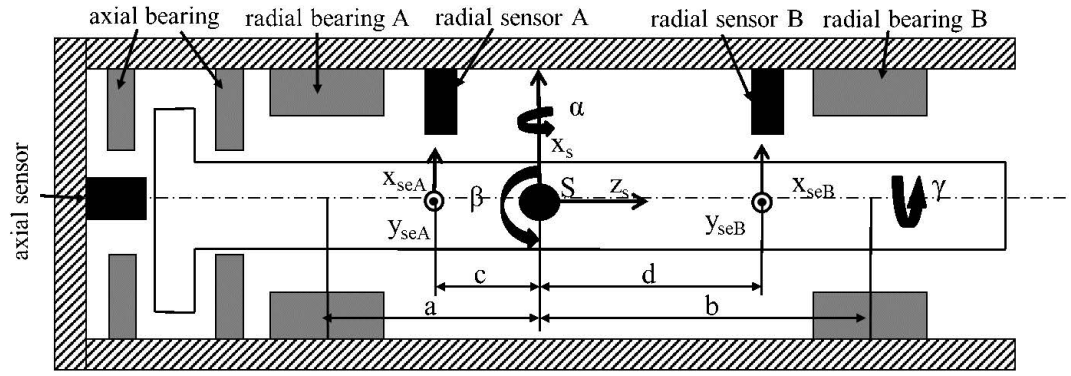

Figure 1. 5-DOF active magnetic bearing (AMB) system.

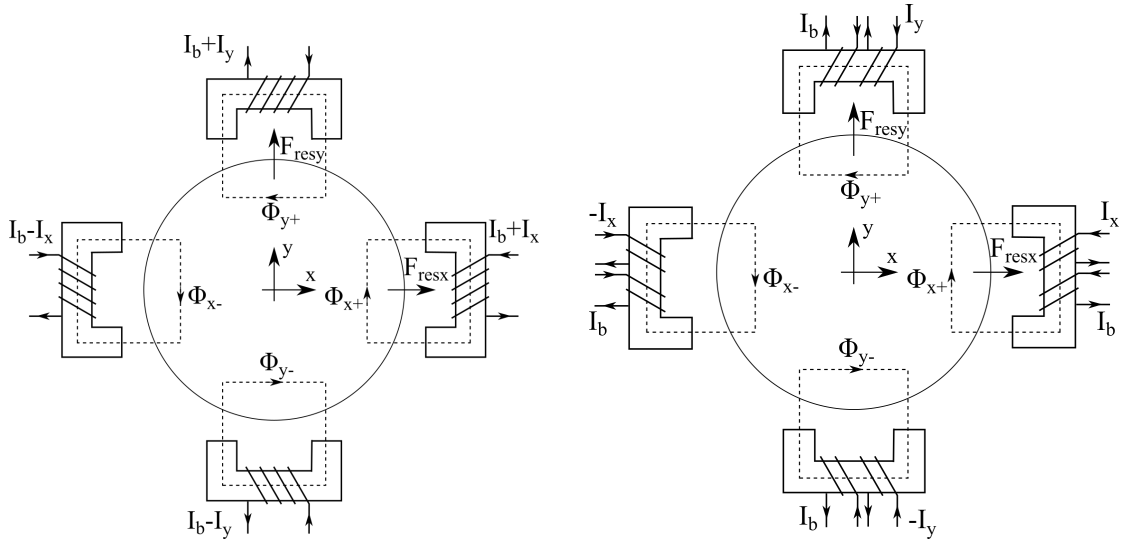

(**a**)Differential driving mode (**b**)Differential winding mode

Figure 2. Force generation in active magnetic bearing systems.

In this paper, the differential driving mode is used for the force generation. Using Ampere's law and Equation (5), the force in x-direction is given as:

$$\mathbf{F}_x = \frac{1}{4}\mu_0 N^2 A_p \left(\frac{(I_b + I_x)^2}{(x_0 - x)^2} - \frac{(I_b - I_x)^2}{(x_0 + x)^2} \right) \tag{6}$$

with the air gap x_0 if the rotor is in the reference position. In Equation (6), it can be seen that the force depends nonlinearly on the force and the current. However, to use the elements of linear control theory, Equation (6) is linearized, and it is assumed that $x_0 >> x$.

$$F_x = \frac{\partial F_x}{\partial I_x} I_x + \frac{\partial F_x}{\partial x} x = \frac{\mu_0 N^2 A_p I_b}{x_0^2} I_x + \frac{\mu_0 N^2 A_p I_b^2}{x_0^3} x = k_i I_x + k_x x \tag{7}$$

The derivation of the force in the y-direction is done in the same way. Combining the equation of the force generation (7) with the basic mechanical Equation (2) leads to the system equation of the magnetic bearing systems:

$$\begin{aligned} \mathbf{M}\ddot{\mathbf{x}} + \mathbf{G}(\omega)\dot{\mathbf{x}} + \mathbf{B}\mathbf{K}_S\mathbf{B}^T\mathbf{x} &= \mathbf{B}\mathbf{K}_i\mathbf{i} \\ \mathbf{y} &= \mathbf{C}\mathbf{x} \end{aligned} \tag{8}$$

with:

$$\mathbf{K}_S = \begin{bmatrix} k_{xa} & 0 & 0 & 0 \\ 0 & k_{xb} & 0 & 0 \\ 0 & 0 & k_{xa} & 0 \\ 0 & 0 & 0 & k_{xb} \end{bmatrix} \mathbf{B} = \begin{bmatrix} a & b & 0 & 0 \\ 1 & 1 & 0 & 0 \\ 0 & 0 & a & b \\ 0 & 0 & 1 & 1 \end{bmatrix} \mathbf{C} = \begin{bmatrix} c & 1 & 0 & 0 \\ d & 1 & 0 & 0 \\ 0 & 0 & c & 1 \\ 0 & 0 & d & 1 \end{bmatrix} \mathbf{y} = \begin{bmatrix} x_{seA} \\ x_{seB} \\ y_{seA} \\ y_{seB} \end{bmatrix} \mathbf{K}_i = \begin{bmatrix} k_{ia} & 0 & 0 & 0 \\ 0 & k_{ib} & 0 & 0 \\ 0 & 0 & k_{ia} & 0 \\ 0 & 0 & 0 & k_{ib} \end{bmatrix} \mathbf{i} = \begin{bmatrix} i_{xA} \\ i_{xB} \\ i_{yA} \\ i_{yB} \end{bmatrix}$$

where k_{xa} and k_{xb} are the linearized negative bearing stiffnesses and k_{ia} and k_{ib} are the linearized force to current factors of the bearings. In Equation (2), only the rigid behavior of the rotor was considered. However, for many industrial applications, also the consideration of the flexible body modes is of great significance. In [6], it was stated that the soft stiffness of magnetic bearings in many applications has a negligible impact on the eigen-frequencies of the flexible modes. Therefore, the flexible eigen-frequencies can be approximately found independent of the control structure. How the flexible body modes are stabilized by the phase shift of the controller is given in [21]. For structures where the stiffness of the magnetic bearing cannot be neglected, the finite element method in combination with the dynamic simulation of the control structure can be used. Finally, it can be stated that it is possible to stabilize the flexible rotor, if the natural frequencies are known for fixed bearing stiffnesses in the whole speed range. Figure 3 shows the flexible behavior of the investigated rotor.

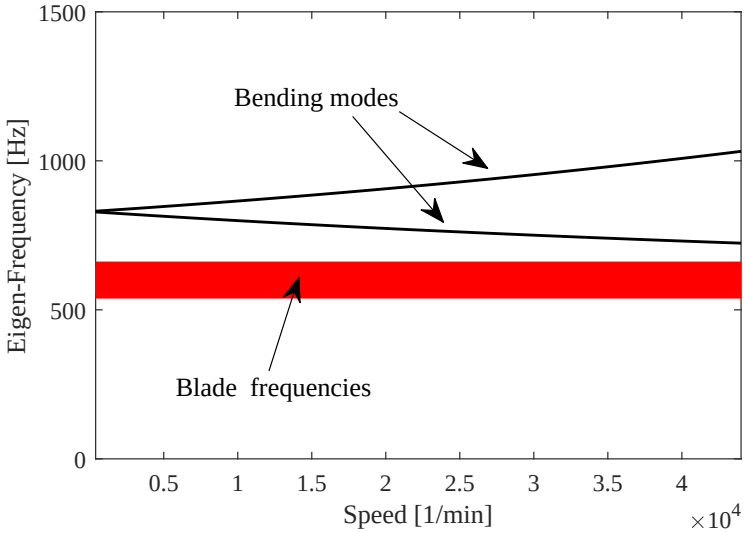

Figure 3. Flexible modes of the considered rotor. Nominal speed is 20,000 rpm.

The first bending modes are in a frequency range where they can destabilize the system. Therefore, the right phase shift has to be guaranteed in this frequency area using additional filters in the control structure. Because the blade frequencies fluctuate for different rotors of the same type and the blade frequencies depend on the rotor speed, the possible occurrence of blade frequencies is marked as a red band. These low resonance frequencies caused by the blade wheel can be destabilized by the control structure.

3. Controller Design

The controller design is based on the rigid body system (8). A computed torque (CT)-based control structure was already designed in [6]. However, this control structure had no problems with low blade frequencies. Different running tests showed that vibrations caused by blade resonances increased to non-acceptable values using only CT-control. Therefore, the first part of this section is the explanation of a CT-based control structure. Afterwards, the control structure is extended for the system with low blade frequencies.

3.1. Input-Output Transformation

In some cases, the tilting and the translation movements are decoupled in Equation (8). In order to use the advantage of this decoupling for other rotor shapes, an input-output transformation is introduced. For this decoupled system, the controller design using the PID controller is a straightforward procedure at standstill.

Figure 4 shows a schematic of the input-output transformation. The following equations are derived under the assumption that the matrices $\mathbf{C}$ and $\mathbf{BK}_i$ are invertible. The input transformation matrix $\mathbf{T}_{in}$ transforms the sensor values $\mathbf{y}$ to the center of gravity (COG)-coordinates $\mathbf{x}$. Thus, the input transformation matrix $\mathbf{T}_{in}$ is given by:

$$\mathbf{T}_{in} = \mathbf{C}^{-1} \tag{9}$$

Using this input transformation, the controller has the COG-coordinates as the input. However, the outputs of the controller are still the actuator currents. In order to design the PID controller in the COG coordinates, also the outputs of the controller are transformed using the output transformation matrix $\mathbf{T}_{out}$:

$$\mathbf{T}_{out} = (\mathbf{BK}_i)^{-1} \tag{10}$$

Using this input-output transformation, the inputs of the PID controllers are the COG coordinates, and the outputs are the forces and torques reduced in the center of gravity. The system equation for the transformed system is given by:

$$\begin{aligned} \mathbf{M}\ddot{\mathbf{x}} + \mathbf{G}(\omega)\dot{\mathbf{x}} + \mathbf{BK}_S\mathbf{B}^T\mathbf{x} &= \mathbf{i}_{COG} \\ \mathbf{y} &= \mathbf{x} \end{aligned} \tag{11}$$

with the transformed current $\mathbf{i}_{COG}$. Now, the coupling of the tilting and translation mode is reduced. However, the term $\mathbf{BK}_S\mathbf{B}^T\mathbf{x}$ still couples the tilting and translation modes. However, this coupling is small compared to the geometrical coupling caused by the input and output matrices in many magnetic bearing systems.

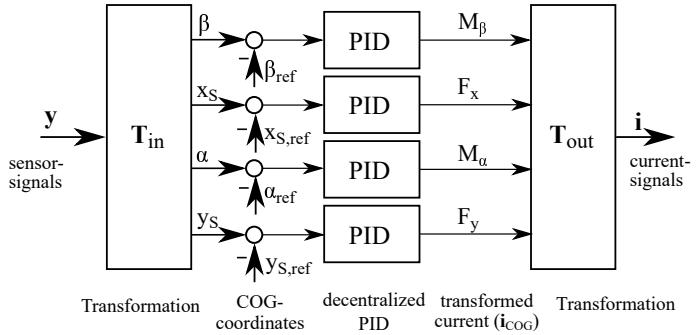

Figure 4. Illustration of the input output transformation.

3.2. Decoupling Using an Inverse Dynamic Approach

The gyroscopic effect $\mathbf{G}(\omega)$ causes problems in the high speed range, because of the split up of the eigen-frequencies (Figure 5) using standard PID controllers.

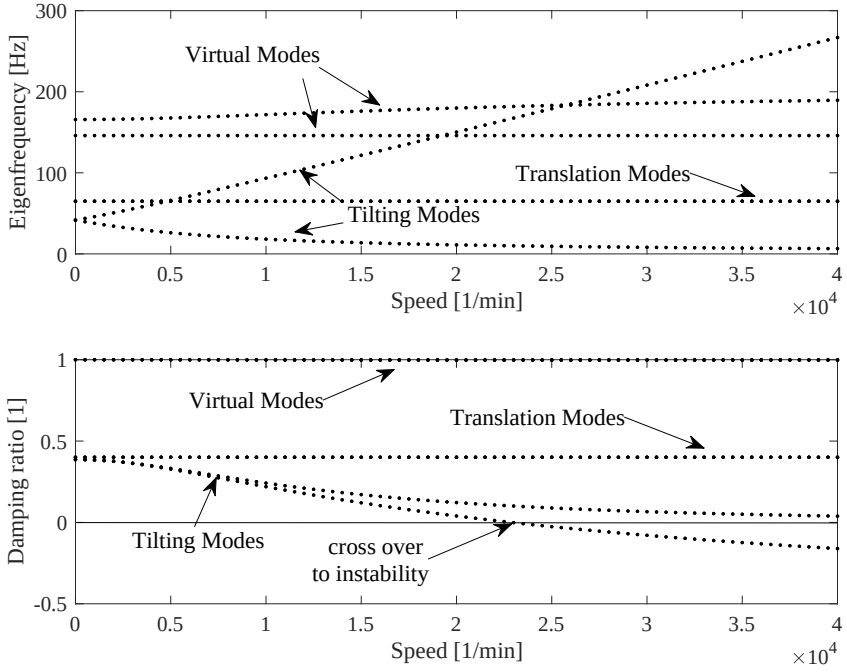

Figure 5. Campbell diagram of a linear time-invariant (LTI)-controlled AMB system.

For a decoupled system according to Equation (11), the speed-variance is only present in the tilting eigen-frequencies. Therefore, the tilting controllers have to ensure a damping action for a high frequency range. With LTI PID controllers, the system can become unstable for a certain speed range according to Figure 5. The virtual modes are eigenvalues of the low pass filter, which are used to limit the differentiating action. The stability can be seen from the damping plot. It is of course possible to design a controller with a very high bandwidth to stabilize the system also in the high speed range. However, this high bandwidth will lead to very high gains and will affect the bending and blade resonance frequencies. To solve this problem, a speed-variant compensation can be developed according to [6,7]. Using the control law:

$$\mathbf{i}_{COG} = \mathbf{v} + \mathbf{G}(\omega)\dot{\mathbf{x}} + \mathbf{B}\mathbf{K}_s\mathbf{B}^T\mathbf{x} \tag{12}$$

the system with the virtual input $\mathbf{v}$ is decoupled and parameter-invariant. For such a decoupled system, a decentralized control procedure:

$$\mathbf{v} = -\mathrm{diag}(f_1(s)...f_4(s))\mathbf{x} \tag{13}$$

shows an acceptable performance, where $f_1(s)...f_4(s)$ are the transfer functions of the decentralized controllers. For commissioning of magnetically-levitated rotors, the peak of the sensitivity function is limited to a factor three according to ISO 14839-3. Using the control approach of Equation (12) directly, this robustness measure is hard to fulfill [6]. To decrease the sensitivity peak, a factor z is introduced, which limits the compensation of the gyroscopic effect. Thus, the complete control law for the rigid body rotor is:

$$\mathbf{i} = \mathbf{T}_{out}\left(\mathbf{v} + z\mathbf{G}(\omega)\dot{\mathbf{x}} + \mathbf{B}\mathbf{K}_s\mathbf{B}^T\mathbf{x}\right) \qquad z \leq 1 \tag{14}$$

Using this control law, the closed-loop system is given by:

$$\mathbf{M}\ddot{\mathbf{x}} + (1 - z)\,\mathbf{G}(\omega)\dot{\mathbf{x}} = \mathbf{v} \tag{15}$$

With the factor z, a trade-off has to be made between the robustness and the required bandwidth of the rigid body controller. To calculate the control law, the velocities of the states $\dot{\mathbf{x}}$ have to be known. It is possible to calculate the velocities using numerical differentiation. However, the noise and the high gain of such simple structures cause problems in the region of the blade or bending modes. Thus, a Kalman filter is used for the estimation of the velocities instead. In order to minimize the controller effort, LTI Kalman filters using the gain scheduling method for the open loop speed variant system were developed. Someone might think the easier way is to gain the schedule decentralized LTI filter for stabilizing the rotor for high speeds. However, the lack of this method is the splitting up of the eigenvalues. Therefore, the separating margin between the rigid body modes and the flexible modes decreases. Another simplification for minimizing the controller effort is that only the stationary solution of the Riccati equation is used, which can be calculated offline. The Kalman filter can be split up in an observer for the tilting movement and an observer for the translation movement according to [6,7]. The estimated states are calculated as follows:

$$\hat{\mathbf{x}}_{Ti,k+1} = \mathbf{\Phi}_{Ti}\hat{\mathbf{x}}_{Ti,k} + \mathbf{\Gamma}_{Ti}\mathbf{v}_{Ti,k} + \hat{\mathbf{K}}\left(\mathbf{y}_{Ti} - \mathbf{C}_{Ti}\hat{\mathbf{x}}_{Ti,k}\right) \tag{16}$$

where the index Ti describes that only the tilting part of the system is used. The feedback matrix $\hat{\mathbf{K}}$ is calculated by an algebraic Riccati equation dependent on the weights of the process error and the sensor noise.

For the reduction of the parameter variance caused by the gyroscopic effect, only the tilting velocities are necessary. Thus, the computing effort is reduced by a factor of four compared to a Kalman observer for the whole system. The high impact of the co-variance matrices on the sensitivity of the system is described in [6].

3.3. Stabilizing the Bending Modes

The controller design procedure of the previous section describes only the stabilization of the rigid body system. In many industrial applications, it is also important to consider the flexible behavior of the rotor. The flexible body modes can be stabilized using second order filters. The phase ϕ in the region of the eigen-frequencies is of great significance [21]. For flexible body modes, the controller provides damping at phase ranges of:

$$0° < \phi < 90° \qquad \text{and} \qquad -180° < \phi < -270° \tag{17}$$

If the separating margin between the flexible modes of the rotor and the rigid body modes is high enough, the bending modes should be stabilized using phases between $-180°$ and $-270°$. This region can be achieved using second order low pass filters. Thus, the gain is decreased in the range of the first bending mode. Figure 3 shows that the separating margin is high enough to stabilize the first bending mode in the phase range between $-180°$ and $-270°$. Experiments showed that the blade frequencies are stable, if the gain of the controller in the range of blade resonances is not too high independent of the phase.

Figure 6 shows the control structure. All parts are explained in the previous section, excluding the unbalance controller. The unbalance controller is a generalized notch filter, which is described in [22], and the speed tracking for the calculation of the unbalance controller is described in [23]. The stabilizing filters are second order low pass filters. The switch at the input of the decentralized PID controller is required to stabilize the blade resonances. For normal operation, the Kalman variables can be used in the whole operating range. However, to show the difference between the feedback using the sensor coordinates and the Kalman variables, the switch is used at a certain speed. The reason for the

stabilization using the Kalman variables instead of the values from the position sensors is described using the controller transfer function (Figure 7).

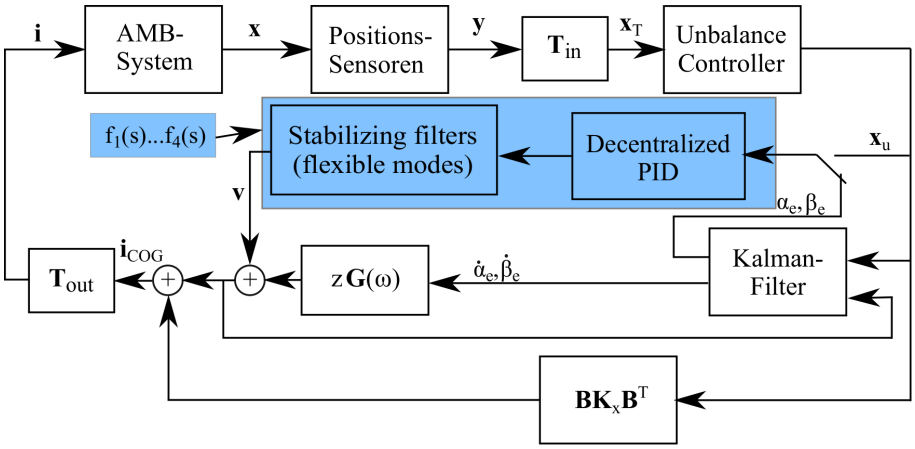

Figure 6. Control structure.

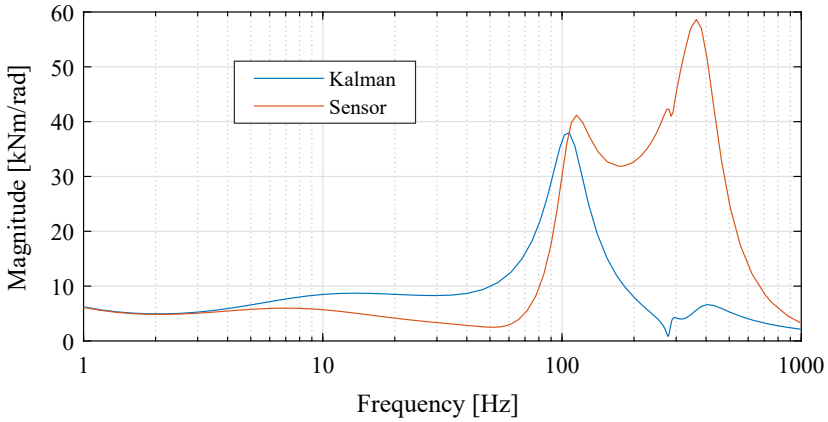

Figure 7. Open loop controller transfer function for the β coordinate of a continuous time simulation.

The gain of the controller in the range of the blade frequencies according to Figure 3 is significantly lower for the system that uses the Kalman coordinates than for the system that uses the sensor variables directly. Because of this low gain, a stable levitation is possible in the desired speed range. The gain plot of the Kalman-based system is strongly affected by the weighting matrices of the Riccati equation. Therefore, a good choice of these matrices is necessary for an acceptable running behavior of the rotor. The weighting matrix $\mathbf{Q}_k$ of the process error and the weighting matrix $\mathbf{R}_k$ of the sensor noise are chosen as diagonal matrices. The entries must not be too high to have a suitable gain in the frequency range of the blade frequencies. In this paper, the diagonal weighting matrices are chosen as follows:

$$\mathbf{Q}_k = \begin{bmatrix} 8 \times 10^6 & 0 & 0 & 0 \\ 0 & 8 \times 10^6 & 0 & 0 \\ 0 & 0 & 8 \times 10^6 & 0 \\ 0 & 0 & 0 & 8 \times 10^6 \end{bmatrix} \tag{18}$$

$$\mathbf{R}_k = \begin{bmatrix} 0.1 & 0 & 0 & 0 \\ 0 & 0.1 & 0 & 0 \\ 0 & 0 & 0.1 & 0 \\ 0 & 0 & 0 & 0.1 \end{bmatrix} \tag{19}$$

In some cases, it could be necessary to use different weights for the translation and tilting movement and different weights dependent on the rotor speed.

For the realization of the controller, a digital Kalman filter is implemented. In order to increase the damping of the digital Kalman-based system, the predicted states $\mathbf{x}_{k+1}$ can be used in some operating ranges. The switch between the sensor coordinates and the predicted states of the Kalman observer are illustrated in Figure 6 at the input of the decentralized PID controller. Figure 8 shows the positive phase shift of the predicted angle β_{k+1} (blue line) to the real angle (black line).

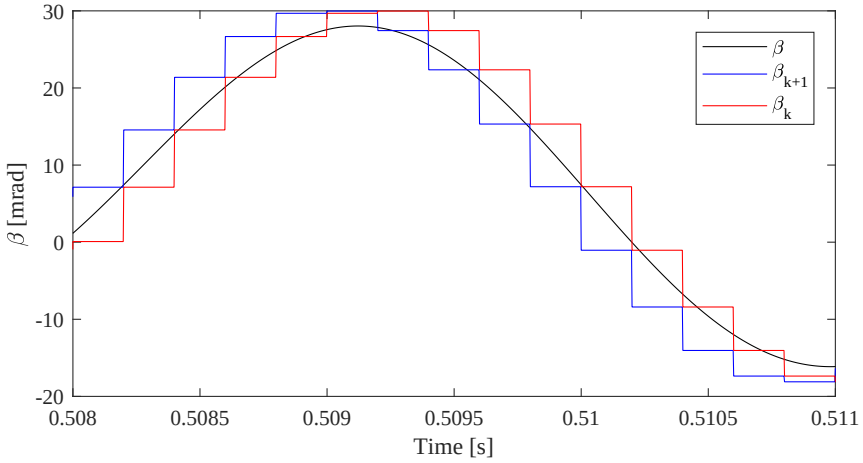

Figure 8. Comparison of the predicted states and the sampled values of the sensors.

If the sensor signal is only sampled, the phase shift is negative, and the damping action of the controller is decreased depending on the sampling frequency (red line). For the reduction of the computational effort, the Kalman observer is only developed for the tilting movement. Therefore, the damping is only increased for the tilting movements. If the damping in the translation coordinates is too low or the measuring and process noise is too high, the Kalman filter can also be extended to the translation coordinates. The usage of the Kalman observer has the advantage of a low gain in the area of the blade frequencies and an increase of the damping compared to the sampled sensor signal.

4. Results

This section shows some experimental results for an industrial system to prove the functionality of the designed control structure. The controller was implemented on a digital signal processor (TMS320DM335) of a state of the art hardware for magnetic bearings. The geometry of the levitated rotor can be seen in Figure 9. The blade wheel is illustrated using the aluminum part (violet part). For the dynamic simulation, the blade wheel was modeled as a rigid part and was fixed on the flexible rotor using a flexible coupling.

The parameters of the explored system are shown in Table 1. The position sensors are inductive sensors, which are excited with a 40 kHz sinusoidal signal. The actuators used the "differential driving mode" for force generation. The data were recorded using a communication protocol between the DSP and the personal computer. Thus, the signals were identical with the variables from the DSP. For the calculation of the predicted states using the Kalman filter, two control cycles were used. Therefore, the sampling time of the Kalman observer was twice the sampling time of the control structure.

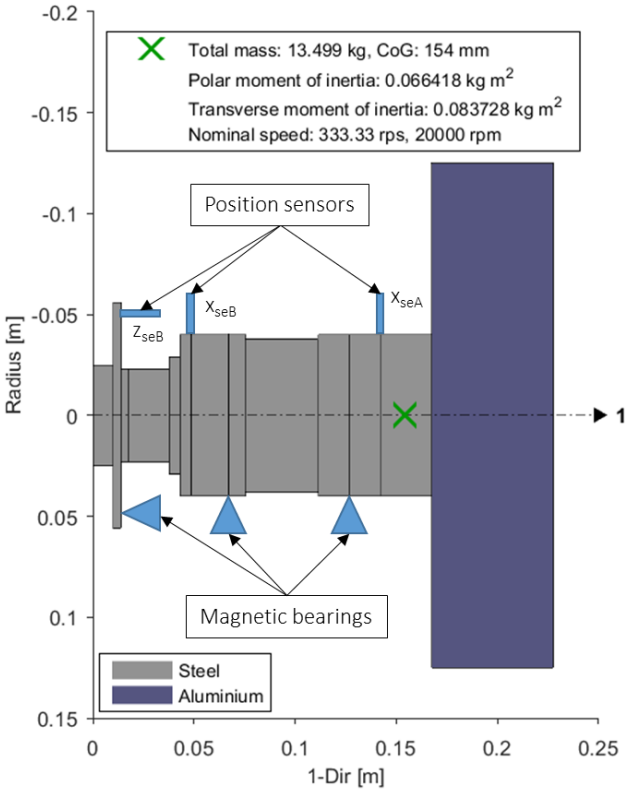

Figure 9. Geometry, sensor and actuator location of the stabilized rotor.

Table 1. System parameters.

Physical Quantity	Symbol	Value
Polar moment of inertia	I_p	0.066418 kg · m^2
Equatorial moment of inertia	I_r	0.083728 kg · m^2
Mass of the rotor	m	13.499 kg
Sampling Time	T_S	100 µs
Sensor bandwidth	BW_S	3.2 kHz
Actuator bandwidth	BW_A	1.3 kHz
Mechanical air-gap	A_G	165 µm
Negative stiffness of the AMB	k_x	120.000 N/m
Force/current factor of the AMB	k_i	110 N/A

4.1. Switching between Controller Inputs

In order to compare the running behavior of the rotor for the estimated tilting coordinates and the sampled coordinates of the sensor signals, the system was investigated around a switching point. The switching point is the time where the input of the controller is changed from the sampled sensor coordinates to the estimated coordinates of the Kalman observer. Figure 10 shows the signal of the position sensor x_{seB} and the current i_{xB}.

The measurement was made at a rotor-speed of about 12,000 rpm. The position signal showed nearly the same behavior for both operations. However, the current signal for the system, which used the sensor directly, had much more noise than the system, which used the predicted variables. For a speed over 12,000 rpm, the system without the predicted states became unstable, because of the high gain in the range of the blade frequencies. Thus, the resonance-frequency caused by the blades was amplified too much, and an unstable feedback system was the consequence. However, for the system that used the predicted states, the gain was low enough that no unstable resonance

occurs. Therefore, the rated speed of 24,000 rpm can be reached using the predicted variables as the controller input.

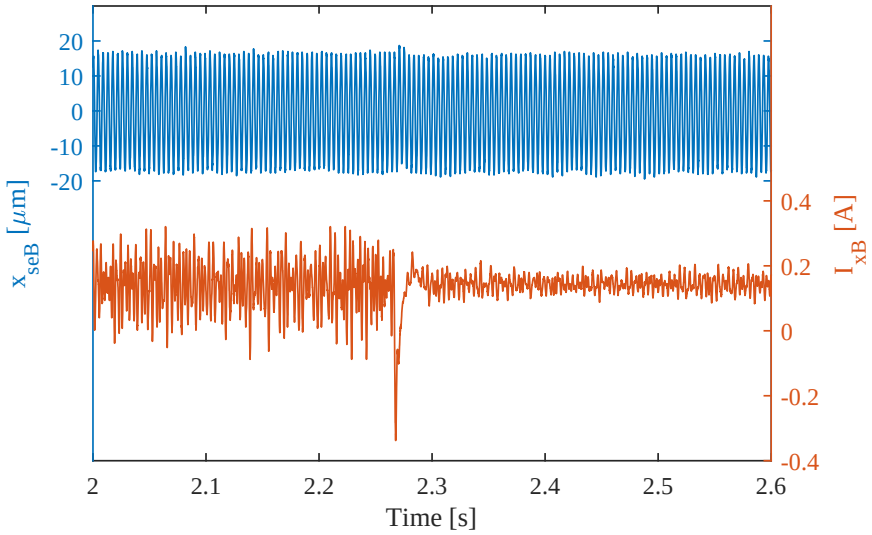

Figure 10. Switching action between the predicted states and the sampled states as input for the position controller.

4.2. Dynamic Behavior at Rated Speed

To describe the dynamical behavior and to get a stability measure, the output sensitivity functions $S(j\omega)$ are used. To evaluate $S(j\omega)$, an excitation e_s on an output $x_{T,i}$ from the transformed output-vector $\mathbf{x_T}$ of the system was used according to Figure 6. $S(j\omega)$ can be calculated with:

$$S(j\omega) = \frac{\mathrm{FFT}(y_i)}{\mathrm{FFT}(e_s)} \tag{20}$$

where FFT means the "fast-Fourier-transformation" of a signal. For an MIMO-system, the sensitivity function becomes a sensitivity matrix. However, according to ISO 14839-3, only the diagonal element of the sensitivity is necessary for the evaluation of the stability. To get a stability measure, the highest peak of the sensitivity function was used. For newly-commissioned magnetically-levitated rotors, the highest peak has to be below a gain of 3 (9.5 dB). The highest peak of the sensitivity function describes the closest distance to the Nyquist point. This closest distance to the Nyquist point implies also limits in the gain and phase margin [24]. For the evaluation of the sensitivity functions, the COG coordinates were used instead of the sensor and bearing coordinates. For these coordinates, the sensitivity function can be separated into two tilting, two translation and one axial sensitivity functions. The impact of the gyroscopic effect should only be present in the tilting sensitivity functions. Because the axial movement was a simple SISO-system, only the sensitivity functions of the tilting and translation movements are shown (Figure 11).

The peak at 400 Hz was caused by the unbalance of the rotor. Thus, this peak was an error in the evaluation of the sensitivity function. Because there was always an output signal independent of the excitation signal, the unbalance peak was not a stability measure of the system. The phase plot of the sensitivity function is not shown, because in order to fulfill the ISO norm, only the magnitude plot is important. The magnetic bearing system had an almost isotropic behavior in the x- and y-direction. Therefore, only one tilting and one translation sensitivity function are shown. The sensitivity functions showed that the ISO 14839-3 was fulfilled. The sensitivity functions for standstill and rated speed showed a similar dynamical behavior. This fact proves the compensation action of the developed control structure.

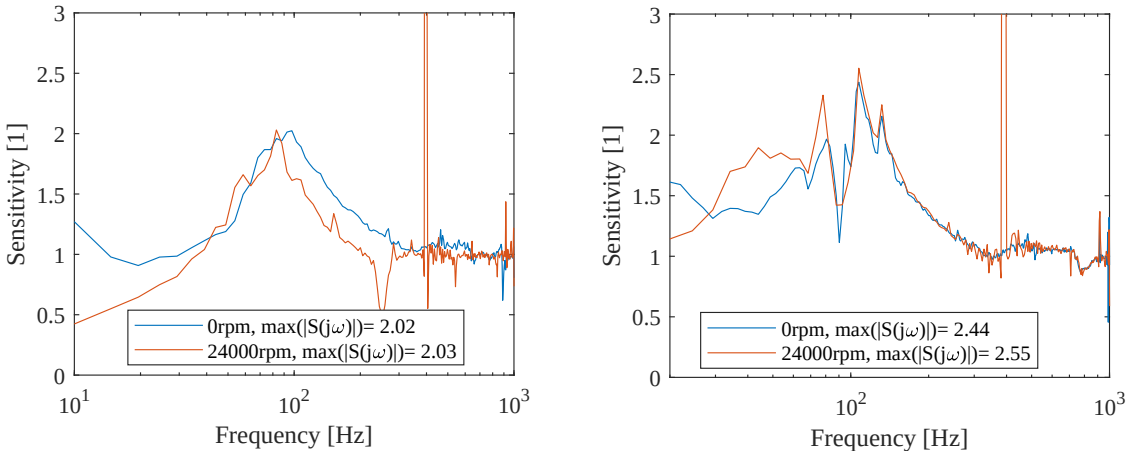

(**a**)Tilting movement (**b**)Translation movement

Figure 11. Sensitivity function at standstill and rated speed.

The next measurements deal with the compliance of the AMB-system. Figure 12 shows the compliance function at rated speed. The compliance functions were also evaluated in the COG coordinates. Thus, one tilting and one translation compliance function were measured. The compliance T_c was evaluated with:

$$T_c(j\omega) = \frac{\mathrm{FFT}(y_i)}{\mathrm{FFT}(e_c)} \tag{21}$$

For the evaluation of the compliance function, the excitation was done at an entry of the transformed input $\mathbf{i}_{COG}$. The values for β and α are given in µrad, and the values for x_S and y_S are given in µm in the DSP.

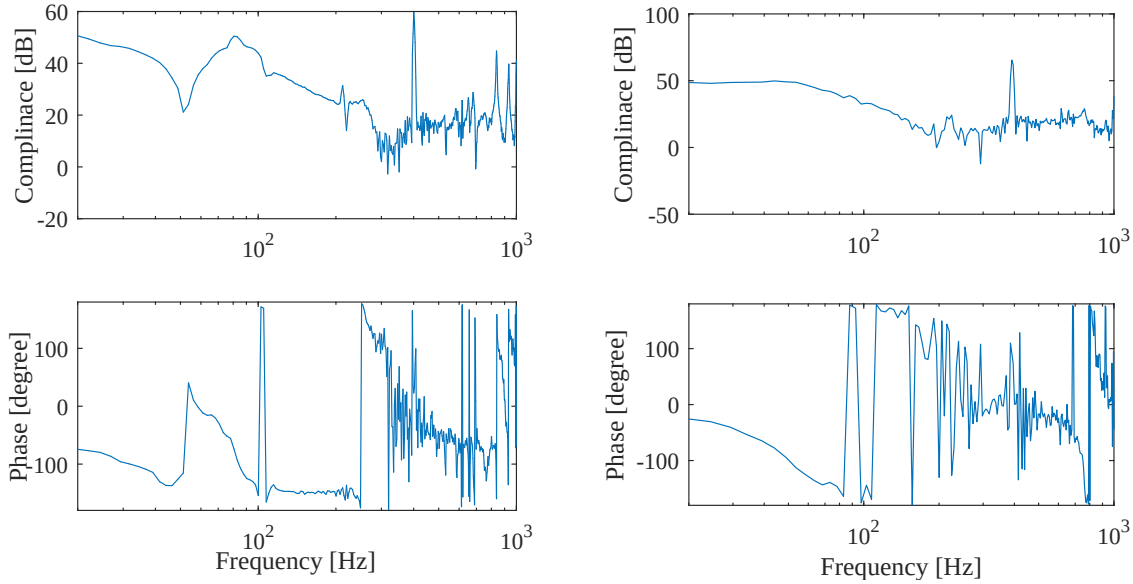

(**a**)Tilting movement (**b**)Translation movement

Figure 12. Compliance function at rated speed.

This choice of the units is the reason for the high gain in the compliance functions. The peak at 400 Hz was again caused by the unbalance frequency. The peaks at around 800 and 900 Hz on the

tilting compliance functions showed the forward and backward whirl first bending modes. However, because of the under-critical operation, these bending modes did not cause problems in the running behavior of the rotor. In the range of the blade frequencies, no peak can be detected. Thus, the control structure had almost no effect on the blade frequencies, because of the reduced gain caused by the Kalman observer.

5. Conclusions

This paper described the controller design for a turbo-molecular pump with low resonance frequencies of the blade wheel and a significant gyroscopic effect. For the stabilization of the rigid body eigen-modes, a controller based on the inverse dynamic of the system was developed. The flexible eigen-modes are stabilized using second order filters. In order to stabilize the resonance frequencies caused by the blade wheel, a Kalman observer is developed. The weighting matrices of the Kalman observer were chosen in a way that the transfer function of the control structure has very low gain in the range of the blade resonances. For the input of the controller, the predicted states for the next sampling point are used to get more damping action depending on the sampling time. The experimental results prove the functionality of the developed control structure. The noise in the frequency range of the resonance frequencies of the blade wheel could be significantly decreased. The sensitivity function of the closed loop system fulfills the ISO 14839-3. Thus, the system has sufficient robustness against disturbances. As a next step, the proposed control structure should be extended and tested for an overcritical rotor.

Acknowledgments: This project was supported by TU Wien in the framework of the Open Access Publishing Program.

Author Contributions: The control structure was developed and tested by Markus Hutterer. Manfred Schrödl supported Markus Hutterer with his expert knowledge and useful discussions for this development.

Conflicts of Interest: The authors declare no conflict of interest.

References

1. Jinji, S.; Jiancheng, F. A novel structure of permanent-magnet-biased radial hybrid magnetic bearing. *J. Magn. Magn. Mater.* **2011**, *323*, 202–208.
2. Hofer, M. Design and Sensorless Position Control of a Permanent Magnet Biased Radial Active Magnetic Bearing. Ph.D. Thesis, TU Wien, Vienna, Austria, 2013.
3. Nenning, T.; Hofer, M.; Hutterer, M.; Schrödl, M. Setup with two Self-Sensing Magnetic Bearings using Differential 3-active INFORM. In Proceedings of the 14th International Symposium on Magnetics Bearings, Linz, Austria, 11–14 August 2014.
4. Garcia, P.; Guerrero, J.; Briz, F.; Reigosa, D. Sensorless Control of Three-Pole Active Magnetic Bearings Using Saliency-Tracking-Based Methods. *IEEE Trans. Ind. Appl.* **2010**, *46*, 1476–1484.
5. Bleuler, H. Decentralized Control of Magnetic Rotor Bearing Systems. Ph.D. Thesis, Federal Institute of Technology Zürich, Zürich, Switzerland, 1984.
6. Hutterer, M.; Schrödl, M. Control of a Flexible Magnetic Levitated Rotor using the Computed Torque Method in Combination with Stabilizing Filters. In Proceedings of the 2016 IEEE International Conference on Advanced Intelligent Mechatronics, Banff, AB, Canada, 12–15 July 2016.
7. Hutterer, M.; Hofer, M.; Schrödl, M. Decoupled Control of an Active Magnetic Bearing System for a High Gyroscopic Rotor. In Proceedings of the 2015 IEEE International Conference on Mechatronics, Nagoya, Japan, 6–8 March 2015.
8. Ahrens, M.; Kucera, L.; Larsonneur , R. Performance of a Magnetically Suspended Flywheel Energy Storage Device. *IEEE Trans. Control Syst. Technol.* **1996**, *4*, 494–502.
9. Nair, S.; Vaidyan, M.; Joy , M. Generalized design and disturbance analysis of robust H infinity control of active magnetic bearings. In Proceedings of the IEEE/ASME International Conference on Advanced Intelligent Mechatronics, Singapore, 14–17 July 2009.

10. Lösch, F.; Gäler, C.; Herzog , R. μ-Synthesis Controller Design for a 3 MW Pump Running in AMBs. In Proceedings of the 6th International Symposium on Magnetics Bearings, Cambridge, MA, USA, 5–7 August 1998.
11. Noshadi, A.; Shi, J.; Lee, W.; Shi, P.; Kalam, A. Robust control of an active magnetic bearing system using H∞ and disturbance observer-based control. *J. Vib. Control* **2017**, *23*, 1857–1870.
12. Pesch, H.; Smirnov, O.; Pyrhonen, W.; Sawicki, J. Magnetic bearing spindle tool tracking through μ-synthesis robust control. *IEEE/ASME Trans. Mechatron.* **2015**, *20*, 1448–1457.
13. Balini, H.; Scherer, C.; Witte, J. Performance enhancement for AMB systems using unstable H∞ controllers. *IEEE Trans. Control Syst. Technol.* **2011**, *19*, 1479–1492.
14. Jastrzebski, R.; Hynynen, K.; Smirnov, A. H∞ control of active magnetic suspension. *Mech. Syst. Signal Process.* **2010**, *24*, 995-1006.
15. Lui, K.; He, R. A nonlinear output feedback control method for magnetic bearing systems. In Proceedings of the European Control Conference, Cambridge, UK, 1–4 September 2003.
16. Tong, W.; Jiancheng, F. A feedback linearization control for the nonlinear 5-dof flywheel suspended by the permanent magnet biased hybrid magnetic bearings. *Acta Astronaut.* **2012**, *79*, 131–139.
17. Darbandi, S.; Behzad, M.; Salarieh, H.; Mehdigholi, H. Linear Output Feedback Control of a Three-Pole Magnetic Bearing. *IEEE/ASME Trans. Mechatron.* **2014**, *19*, 1323–1330.
18. Schmidt, R.M.; Schitter, G.; Eijk, J. *The Design of High Perfromance Mechatronics*; Delft University Press: Delft, The Netherlands, 2014; ISBN 978-1-61499-367-4.
19. Schweitzer, G.; Maslen, E. *Magnetic Bearings*; Springer: Berlin, Germany, 2009; ISBN 978-3-642-00496-4.
20. Hofer, M.; Schmidt, E.; Schrödl, M. Design of a Three Phase Permanent Magnet Biased Radial Active Magnetic Bearing Regarding a Position Sensorless Control. In Proceedings of the 2009 Twenty-Fourth Annual IEEE Applied Power Electronics Conference and Exposition, Washington, DC, USA, 15–19 February 2009.
21. Schmied, J.; Kosenkov, A. Practical controller design for rotors on magnetic bearings by means of an efficient simulation tool. In Proceedings of the 10th International Conference on Vibrations in Rotating Machines, San Antonio, TX, USA, 3–7 June 2013.
22. Herzog, R.; Bühler, P., Gähler, C. Unbalance Compensation Using Generalized Notch Filters in the Multivariable Feedback of Magnetic Bearings. *IEEE Trans. Control Syst. Technol.* **1996**, *4*, 580–586.
23. Hutterer, M.; Kalteis, G., Schrödl, M. Redundant unbalance compensation of an active magnetic bearing system. *Mech. Syst. Signal Process.* **2017**, *94*, 267–278.
24. Skogestad, S.; Postlethwaite, I. *Multivariable Feedback Control: Analysis and Design*; Wiley: New York, NY, USA, 2005; ISBN 978-0-470-01167-6.

© 2017 by the authors. Licensee MDPI, Basel, Switzerland. This article is an open access article distributed under the terms and conditions of the Creative Commons Attribution (CC BY) license (http://creativecommons.org/licenses/by/4.0/).